Response to RC1:

This paper focuses on the atmospheric CO_2 dynamics in Guangzhou, a coastal megacity. It does this by developing an observation-based framework that integrates ground-based CO and CO_2 observations, as well as $\Delta CO/\Delta CO_2$ ratios. The paper analyses the spatiotemporal patterns of CO_2, assesses the influence of sea–land breezes and partitions anthropogenic and biogenic emissions. While the study presents interesting findings regarding Guangzhou's carbon emissions, some clarification of the results is necessary. The manuscript could be improved by providing more comprehensive interpretations of the methods and results, particularly with regard to the uncertainty of the results presented. Please see my comments below.

Response:

We appreciate the reviewer for the constructive overview and insightful suggestions, which have been very helpful in improving the quality of the manuscript. Guided by these comments, we have revised the manuscript to improve the clarity and rigor of the methods and results and to better communicate uncertainties and limitations where relevant. Below we provide point-by-point responses and indicate the exact locations where the corresponding revisions were implemented in the revised manuscript. The revised text has been highlighted in the manuscript for ease of reference.

General Comments:

(1) CO was measured simultaneously, but is only analysed in Section 3.4. Since CO is a good proxy for CO_2 over urban regions, it would be interesting to check the CO results, for example in Figures 4 and 6. Please show and interpret the diurnal cycle of CO in contrast to CO_2.

Response:

We agree that CO provides an important combustion tracer to interpret CO_2 variability. To directly address this, we added two new supplemental figures and concise cross-species interpretation in the main text. Specifically, we now show (i) synchronous CO diurnal cycles across seasons and weekdays/weekends for NS, PY and CH (new Fig. S9), and (ii) CO diurnal cycles during SLB days versus non-SLB days at NS (new Fig. S11) to complement the CO_2 results in Figs. 5 and 7 (formerly Figs. 4 and 6). We kept Figs. 5 and 7 focused on CO_2 to avoid overcrowding, but we added explicit caption cross-references to Figs. S9 (Line 438) and S11 (Lines 510–511) and summarized the key contrasts in Sect. 3.1.2 (Lines 464–473) and Sect. 3.2 (Lines 512–520).

In these added texts, we highlight three robust CO–CO_2 contrasts: (1) the morning CO peak aligns with the CO_2 morning maximum at PY (combustion/traffic influence), (2) CO lacks a pronounced mid-afternoon minimum (supporting biogenic control of the CO_2 midday drawdown), and (3) CO confirms the seasonally opposite SLB regimes (ventilation in cooler seasons vs summertime trapping/recirculation). For consistency, we made corresponding brief updates in the Abstract and Conclusions to note this added CO–CO_2 contrast (Lines 23–26; Lines 733–738).

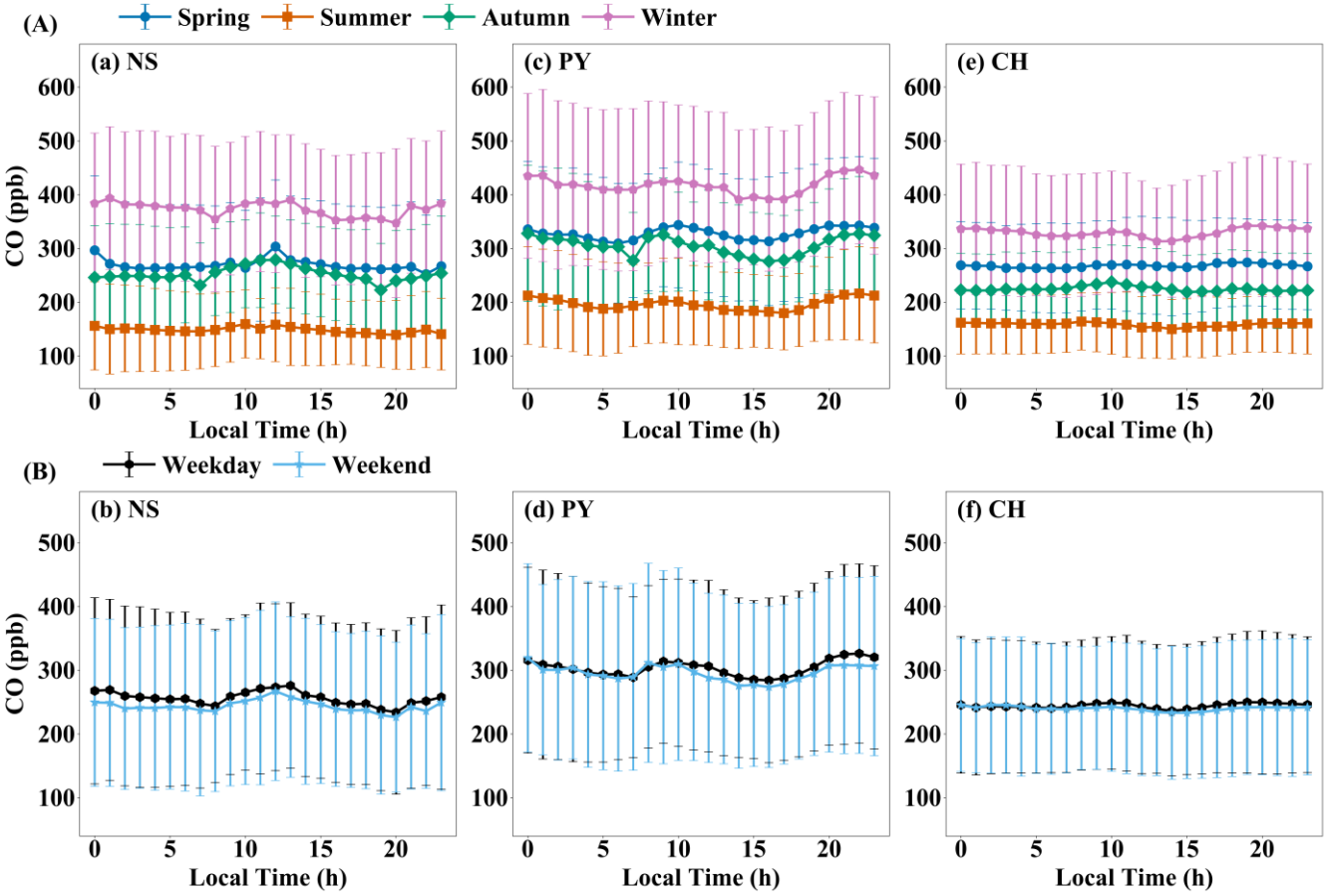

Figure S9. Diurnal CO variations at the (a–b) NS, (c–d) PY, and (e–f) CH stations across (A) seasons and (B) weekdays/weekends. Seasons are defined as Spring (Mar–May), Summer (Jun–Aug), Autumn (Sep–Nov), and Winter (Dec–Feb). Error bars indicate ± 1 SD.

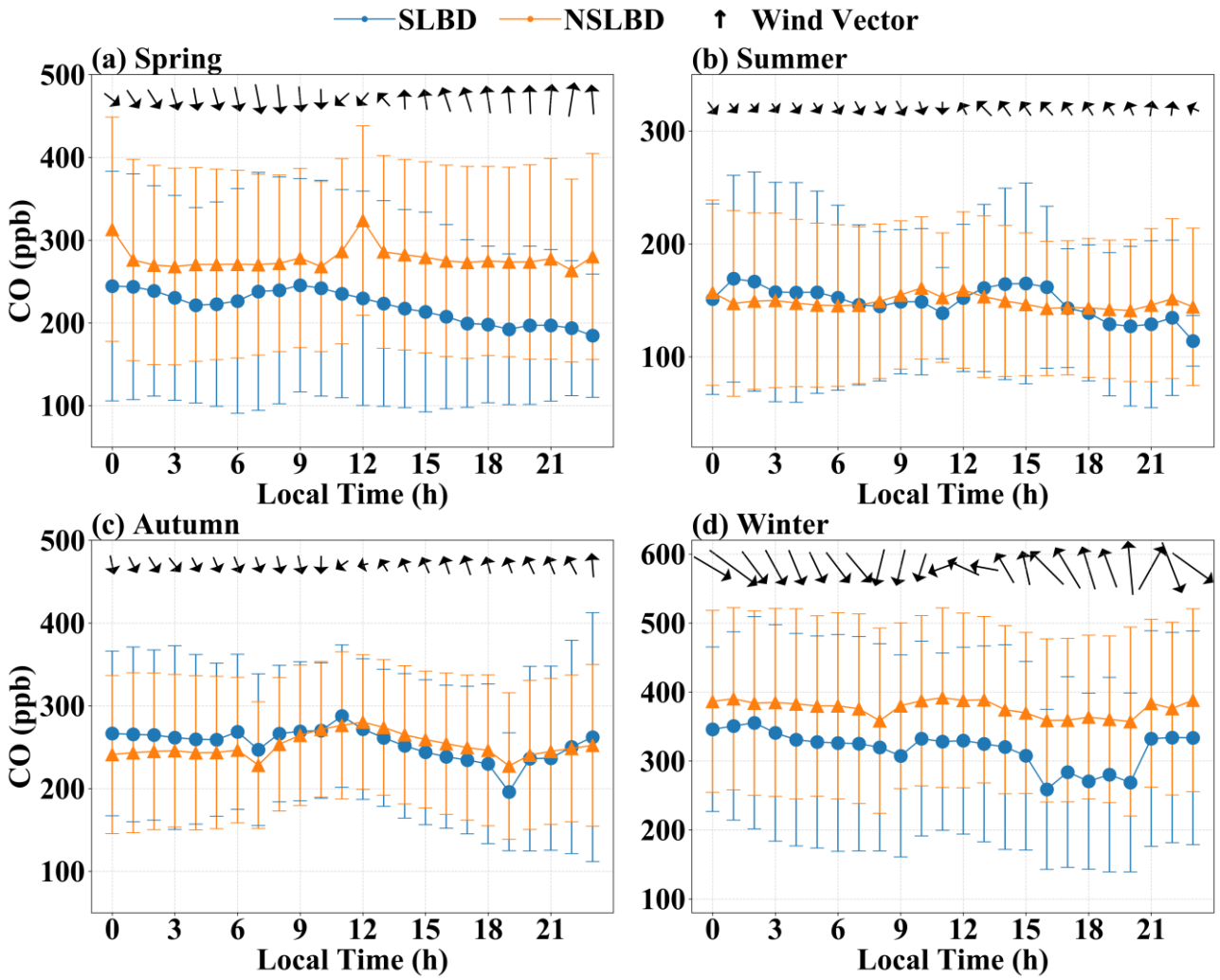

Figure S11. Diurnal variations in CO concentrations, wind direction, and wind speed at the coastal station (NS) during sea–land breeze days (SLBD) and non-SLB days (NSLBD) by season. Error bars indicate ± 1 SD.

(2) Please explain how the error bars in Figure 9 are calculated. It seems to me that the uncertainty is so large that the difference between summer and winter is not significant. Also, what is the uncertainty of the estimation in line 434 (60.17%)?

Response:

We appreciate the reviewer's question about the error bars in Fig. 10 (formerly Fig. 9) and the uncertainty of the reported summertime offset fraction. Figure 10 summarizes afternoon (12:00–16:00 LT) daily means at PY for July 2023 (summer; n = 29 valid days) and December 2023 (winter; n = 18 valid days). For each valid day, we first computed the 12:00–16:00 mean CO_2tot, CO_2ff, and CO_2bio, and then formed the monthly statistics from these daily afternoon means (bars: monthly mean; error bars: ±1 SD across daily means). Thus, the error bars represent day-to-day atmospheric variability in the daily afternoon means—driven mainly by transport/ventilation—rather than the uncertainty of the monthly mean. December has fewer valid days because incomplete-afternoon days (e.g., instrument

downtime/maintenance) were excluded by objective QC; minor numerical differences from the original submission reflect consistent application of this valid-day criterion and do not affect the conclusions (e.g., December CO_2ff mean ± SD: 13.62 ± 9.38 originally vs 13.56 ± 10.17 here).

Because SD reflects variability (not mean uncertainty), overlap of ± 1 SD ranges does not imply that the July–December contrast is insignificant. To directly address significance, we now report the standard error (SE) and 95 % CI of the monthly means and formal comparisons based on daily means (new Table S5). These show that the winter–summer differences remain statistically detectable for CO_2tot, CO_2ff, and CO_2bio (Welch test; p values reported in Table S5), with consistent inferences from Mann–Whitney tests and bootstrap confidence intervals. We also report robust distributional metrics (median and IQR), which corroborate this significant seasonal increase despite partial day-to-day overlap (Table S5).

The "60.17 %" in the original manuscript denotes the summertime biogenic offset fraction, defined as $|CO_2bio|/CO_2ff$ using July afternoon monthly means. Using the harmonized Fig. 10 values, the offset is $|-3.59|/5.97 = 0.6013$ (60.13 %). We quantify its uncertainty using bootstrap resampling of paired daily (CO_2ff, CO_2bio) values (preserving their covariance), yielding 60.13 % with a 95 % CI of 48–72 %.

These clarifications and updates have been implemented in the revised Fig. 10 caption (Lines 635–640) and in Sect. 3.5 (Lines 610–633). The significance testing, SE, and 95 % confidence intervals for the July–December contrasts are summarized in Table S5, while the summertime offset uncertainty (bootstrap 95 % CI of 48–72 %) is reported in Sect. 3.5 (Lines 705–708). For completeness, we briefly note these uncertainty updates in the Conclusions (Lines 746–749).

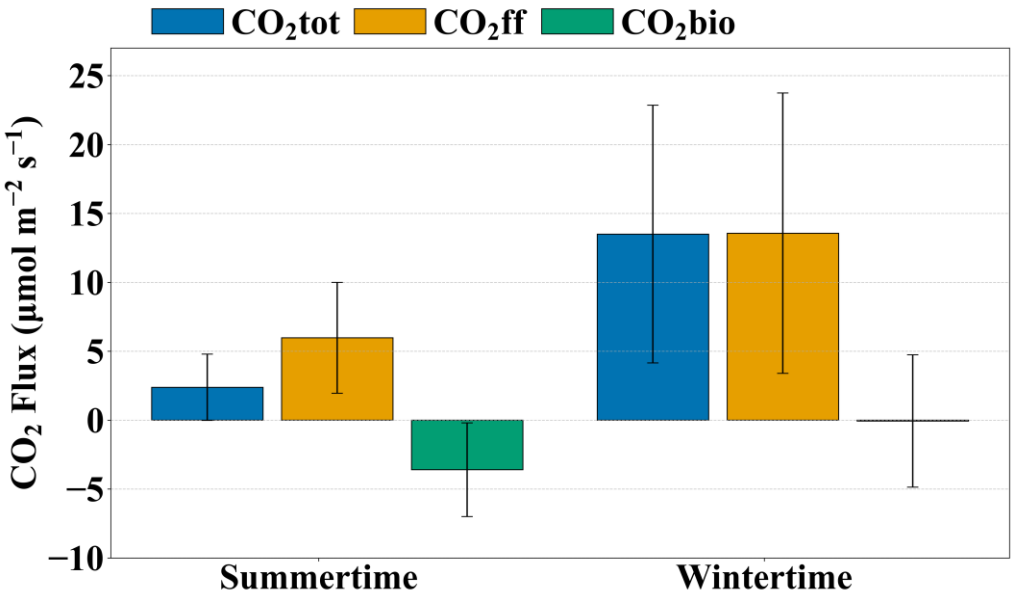

Figure 10. Average afternoon (12:00–16:00 LT) CO_2tot, CO_2ff, and CO_2bio at PY for July 2023 (summer; n = 29 valid days) and December 2023 (winter; n = 18 valid days). December has fewer valid days because objective QC excluded days with incomplete afternoon coverage (e.g., instrument downtime/maintenance), so the smaller winter

sample reflects data availability rather than subjective selection. Bars show monthly means of daily afternoon values. Error bars indicate ± 1 standard deviation (SD) across daily afternoon means within each month (day-to-day atmospheric variability), not the standard error (SE) of the monthly mean; SE and confidence intervals are reported in Table S5.

Table S5. July–December contrasts in daily afternoon means (PY, 12:00–16:00 LT). (Δ = winter − summer; units: μmol m^{-2} s^{-1})

Component	July Mean ± SE	Dec Mean ± SE	July → Dec (median, IQR)	Δ (Welch 95 % CI)	Welch p	Mann–Whitney p	Bootstrap 95 % CI of Δ
CO_2tot	2.38 ± 0.45	13.50 ± 2.20	2.00 (0.72–3.05) → 10.34 (7.16–15.00)	+11.12 [6.40, 15.83]	9.83×10^{-5}	4.06×10^{-7}	[7.10, 15.67]
CO_2ff	5.97 ± 0.75	13.56 ± 2.40	4.33 (3.58–7.81) → 10.70 (6.74–18.28)	+7.59 [2.36, 12.82]	0.0066	0.002	[3.09, 12.65]
CO_2bio	−3.59 ± 0.63	−0.06 ± 1.13	−3.17 (−5.42–−1.39) → −0.20 (−2.11–2.59)	+3.53 [0.87, 6.19]	0.011	0.003	[1.01, 6.04]

(3) The manuscript identifies sea–land breeze (SLB) days based on 24-hour wind direction transitions and a wind speed threshold of <10 m s^{-1}. While this threshold excludes most strong winds, the authors should clarify whether the potential influence of tropical cyclones or their peripheral circulations was considered. Even when wind speeds remain below 10 m s^{-1}, such events can disrupt local wind directions, potentially disturbing the regular daytime–night-time SLB pattern. Without addressing these effects, SLB identification and subsequent CO_2 dynamics interpretation may be biased.

Response:

We appreciate the reviewer's careful comment and agree that tropical cyclones (TCs) or their peripheral circulations could disrupt local wind-direction reversals even under moderate winds. We have implemented these clarifications in Sect. 2.4 (Lines 218–241), where we also note that excluding the single overlapping day does not alter our SLB–CO_2 interpretation, and we summarize the TC screening in Table S2 (new). We address this in three ways:

1) Clarifying the wind-speed threshold (wording vs. implementation). We agree that our original wording "daily mean wind speed < 10 m s^{-1}" could be interpreted ambiguously. We have revised Sect. 2.4 to state explicitly that the <10 m s^{-1} criterion is applied to hourly winds over the entire candidate SLB day (00:00–23:00 LT), i.e., no hourly wind-speed value exceeds 10 m s^{-1}. Importantly, this hourly cap was already used in our original SLB-day classification; the revision corrects the description for

transparency. Reapplying the clarified criteria reproduces the same SLB-day calendar (number and dates unchanged).

2) Two-phase (night/day) requirement and local-wind direction. Our SLB definition requires both a night-time land-breeze phase (01:00–09:00 LT; 302–45°) and a daytime sea-breeze phase (12:00–20:00 LT; 112–202°), each persisting for ≥4 h (or ≥4 h within any running 5 h window). Directional persistence is evaluated using the local-wind direction (after removing the daily-mean background vector), while the wind-speed screen is applied to the observed wind-speed magnitude at 48 m. Together, these requirements reduce the likelihood of misclassifying strongly forced days, because synoptic/TC-peripheral regimes often impose a prolonged anomalous wind pattern rather than a clean diurnal reversal (Atkins and Wakimoto, 1997; Allouche et al., 2023).

3) Targeted TC screening. To explicitly assess residual TC contamination, we cross-referenced the SLB-day calendar against 2023 Pearl River Delta (PRD)/Guangzhou TC impact windows compiled from the official Guangdong–Hong Kong–Macao Greater Bay Area (GBA) Climate Monitoring Bulletin (new Table S2). For each TC, Impact Start/End are defined as the first/last local dates on which the bulletin reports PRD/Guangzhou impacts or advisories attributable to that system (including peripheral rainbands/gusts). Because the bulletin is date-based, we conservatively treat the entire day within each window as potentially TC-influenced. Only one SLB day (2 Sep 2023) overlaps these windows; excluding it leaves results unchanged.

Overall, these revisions clarify the wind-speed screening implementation and explicitly assess potential TC/peripheral influences on SLB identification, indicating no bias in the identified SLB-day set or the associated CO_2 interpretation.

Atkins, N. T. and Wakimoto, R. M.: Influence of the synoptic-scale flow on sea breezes observed during CaPE, Monthly weather review, 125, 2112-2130, https://doi.org/10.1175/1520-0493(1997)125<2112:IOTSSF>2.0.CO;2, 1997.

Allouche, M., Bou-Zeid, E., and Iipponen, J.: The influence of synoptic wind on land–sea breezes, Quarterly Journal of the Royal Meteorological Society, 149, 3198-3219, https://doi.org/10.1002/qj.4552, 2023.

Table S2. Summary of 2023 tropical cyclones (TCs) and impact windows in the Pearl River Delta (PRD)

TC Number	International Name	Impact Start	Impact End	PRD / Guangzhou Impacts (summary)	Primary Reference
2304	Talim	2023-07-15	2023-07-18	Gusty winds and storm surge along the western PRD; strong winds and squally showers in Guangzhou on Jul 17.	2023 Guangdong–Hong Kong–Macao Greater Bay Area (GBA) Climate Monitoring Bulletin (https://my.weather.gov.hk/en/wxinfo/pastwx/2023/files/GD_HK_Mac_GBA_2023.pdf)
2305	Doksuri	2023-07-24	2023-07-29	Peripheral rainbands and thunderstorms; local advisories issued in PRD/Guangzhou.	
2309	Saola	2023-09-01	2023-09-03	Severe gales and heavy rain across PRD; service suspensions; multiple warnings in Guangzhou and surrounding cities.	
2311	Haikui	2023-09-05	2023-09-11	Remnant low brought prolonged heavy rain in PRD; locally record-breaking September rainfall in parts of Guangdong.	
2314	Koinu	2023-10-05	2023-10-09	Sustained gales and heavy rain in PRD; transport/service disruptions; multiple warnings in Guangzhou.	
2316	Sanba	2023-10-19	2023-10-20	Peripheral effects in PRD with rain/gusts; main impacts over western Guangdong (Zhanjiang/Maoming) and Hainan.	

Other Comments:

Although the introduction highlights three key knowledge gaps in the existing research, it does not emphasise their relevance to coastal cities enough, nor does it distinguish these gaps from those in studies of inland cities. Further descriptions are required. While the introduction mentions Guangzhou's GDP, population, green coverage and sea–land breeze frequency, it does not link these to the study objectives. Green coverage, which is important for biogenic fluxes, is neither compared with that in other coastal cities nor discussed in terms of its impact on flux magnitude. The frequency of the sea–land breeze is cited without detailing its seasonal patterns or how it differs from that in other cities. Furthermore, Guangzhou's carbon mitigation policies, which could influence anthropogenic and biogenic CO_2 emissions, are not mentioned.

Response:

Thanks for the constructive and detailed comments. We have revised and partially restructured the Introduction to strengthen the coastal relevance of the three knowledge gaps, explicitly distinguish coastal from inland regimes, and link Guangzhou's city characteristics and policy context directly to our study

objectives.

1) Coastal relevance and coastal-inland distinction. We added explicit language that coastal megacities face attribution challenges driven by land–sea contrasts, marine background inflow, and diurnal reversals in advection/boundary-layer structure, and we contrast this with typical inland regimes lacking marine inflow–outflow (Introduction; Lines 46–52; Lines 76–81).

2) SLB frequency: seasonal patterns and cross-region contrasts. We expanded the SLB description to include its seasonal dependence in the Pearl River Estuary. We also added a concise comparison with other Chinese coastal regions (e.g., the Bohai Rim and Yangtze River Delta) to underscore regional heterogeneity in mesoscale transport and background-wind control (Introduction; Lines 74–76; Lines 81–84).

3) Green coverage: cross-city comparison and implication for flux magnitude. We added a short cross-city comparison of reported built-up-area green coverage among major Chinese coastal megacities (e.g., Guangzhou, Shenzhen, Qingdao, and Tianjin) and explicitly state the implication that biogenic exchange can be non-negligible when interpreting urban observations, with brief supporting examples from the literature (Introduction; Lines 95–105).

4) Explicitly framing the three gaps for coastal settings and distinguishing from inland regimes. We rewrote the three "knowledge gaps" to be explicitly coastal-focused (including SLB-driven transport/mixing and representativeness issues) and to distinguish them from inland-city regimes (Introduction; Lines 107–112). We restate these coastal-focused gaps at the start of the Conclusions for continuity (Lines 717–718).

5) Linking Guangzhou indicators and policy context to the objectives. We revised the Guangzhou context so that GDP/population, greening, and frequent SLB are no longer purely descriptive; instead, together with a brief mitigation-policy framing (e.g., Guangdong ETS and key sector measures), they are explicitly tied to the three coastal-focused gaps and used to motivate our objectives and observation-driven framework for robust source–sink attribution in a policy-relevant coastal megacity setting (Introduction; Lines 112–139). To reflect this framing, we updated the Abstract and Conclusions to more explicitly state the mitigation relevance (Lines 29–31; Lines 761–770).

Line 25: clean air policies? Please provide a little bit more details of these policies in the abstract.

Response:

Thanks for the comment. We revised the Abstract and expanded the policy context in the main text

(Sect. 3.4) to make the "clean-air policies" reference more concrete while keeping claims proportionate to our evidence and within the Abstract word limit.

1) Abstract update. We replaced the generic phrase with a compact sector-level description, stating that the regression-derived R_{CO} is consistent with the reported post-2013 tightening of coal/industrial and vehicle-emission controls (Lines 26–27). For consistency, we made a matching wording edit in the Conclusions (Lines 725–727).

2) Main-text expansion. We added specific programmes and sector measures (coal/power and vehicle controls, including ULE retrofits and China 6 standards) and supporting context, and we explicitly frame this as a consistency check rather than causal attribution, noting other possible contributors (fuel mix, fleet composition, atmospheric oxidation) (Sect. 3.4; Lines 572–581; Lines 587–588).

Line 114: EDGAR full name.

Response:

Thanks for pointing out our mistake. We have revised this in Lines 158–159.

Figure 8: Please show the density plot; the points may overlap strongly with each other.

Response:

Thanks for the suggestion. To reduce overplotting and better visualize the distribution, we revised Fig. 9 (formerly Fig. 8) by replacing the scatter with a 2D histogram density plot (hist2d; 200 × 200 bins), with color indicating the number of paired observations per bin (see colorbar). This highlights the high-density core and sparse tails while retaining the full dataset. Regression lines and reported slope/correlation statistics are computed from the underlying paired data and are unchanged. We updated Fig. 9 and its caption accordingly (Lines 565–569).

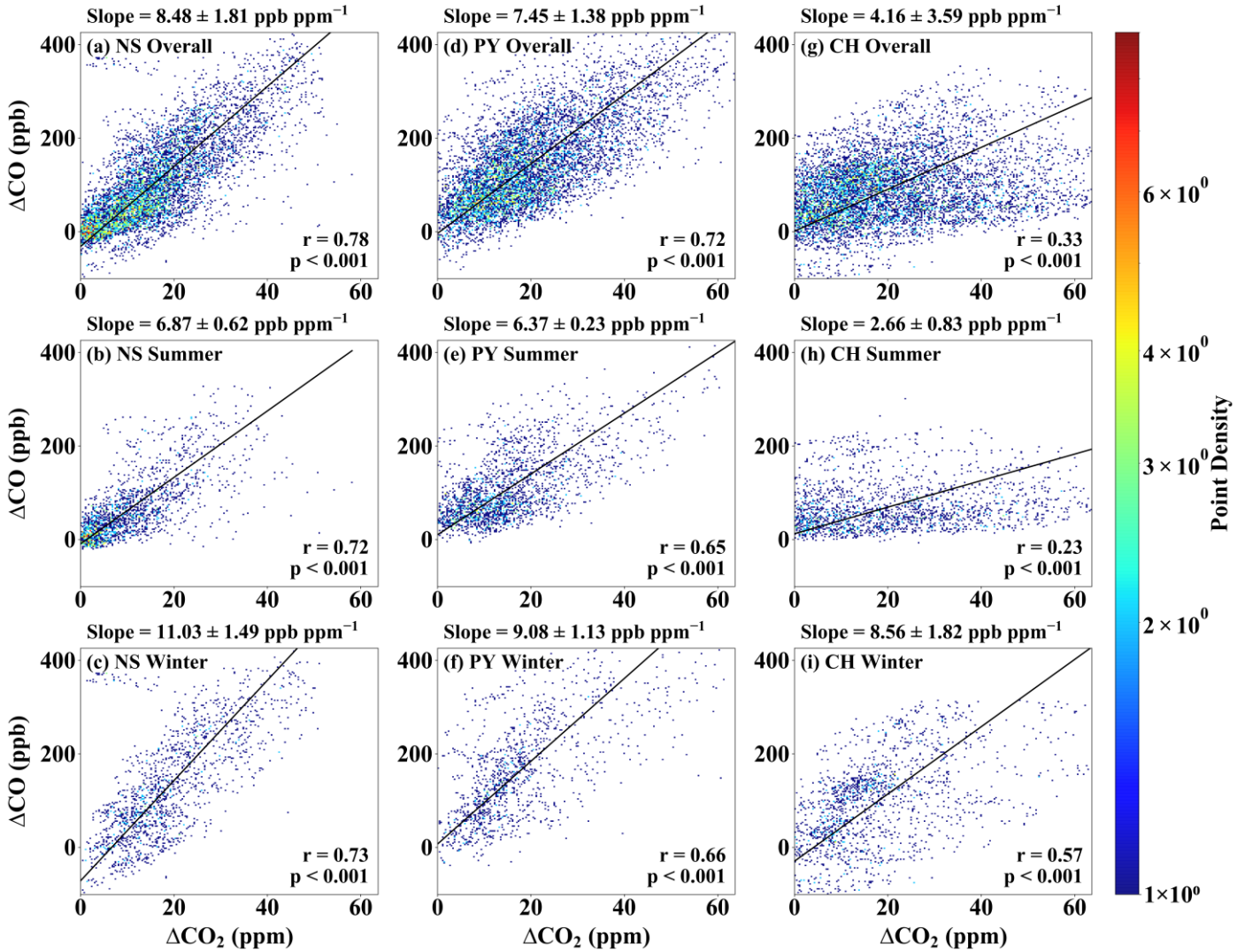

Figure 9. Seasonal relationships between ΔCO_2 and ΔCO enhancements at the (a–c) NS, (d–f) PY, and (g–i) CH stations, analyzed using geometric-mean regression. Panels are shown as 2D histogram density plots (hist2d; 200 × 200 bins), where color indicates the number of paired observations per bin. The fitted slope represents the $\Delta CO/\Delta CO_2$ emission ratio (R_{CO}; ppb ppm^{-1}), reported as mean ± 1 SD (reflecting temporal variability).

Line 448: is the EDGAR mean yearly or monthly? How is the temporal resolution of EDGAR done? How are daytime and night-time emissions differentiated?

Response:

Thanks for your careful comment. The EDGAR product used here is the annual 2023 gridded inventory at 0.1° × 0.1° (EDGAR_2024_GHG; Crippa et al., 2024). To obtain sub-daily variability and distinguish daytime versus nighttime emissions, we temporally disaggregated the annual totals to an hourly series using the high-resolution temporal profiles of Crippa et al. (2020). Daytime/nighttime (and winter-afternoon 12:00–16:00 LT) values are computed by selecting and averaging the corresponding local-time hourly bins. We describe this processing and report the resulting winter-afternoon benchmark over the footprint-defined sensitivity region (Fig. 12) in Sect. 3.5 (Lines 672–675).

Crippa, M., Solazzo, E., Huang, G., Guizzardi, D., Koffi, E., Muntean, M., Schieberle, C., Friedrich, R., and Janssens-Maenhout, G.: High resolution temporal profiles in the Emissions Database for Global Atmospheric Research, Scientific Data, 7, https://doi.org/10.1038/s41597-020-0462-2, 2020.

The STILT model releases 500 particles with a 72-hour backward trajectory and a spatial resolution of 0.08° × 0.08°, but no sensitivity tests are reported. It is unclear whether increasing the number of particles or improving the spatial resolution would significantly affect the footprint simulations. These model parameters directly impact the accuracy of CO_2 emission estimates, so relevant validation analyses are essential.

Response:

Thanks for highlighting the need to document sensitivity to STILT parameters. We agree and have added a targeted winter paired-day sensitivity analysis at PY to quantify how STILT setup choices affect inferred fluxes. Starting from the baseline configuration (500 particles, 0.08° grid, 72 h backward), we independently varied (1) particle number (1000, 2000), (2) grid resolution (0.05°, 0.10°), and (3) backward duration (96 h, 120 h). For each variant we recomputed footprints, reran the flux-estimation workflow, and compared against the baseline using paired daily afternoon means (12:00–16:00 LT; n = 18) with effect sizes (percent/absolute differences), Pearson r, and 95 % CIs (with paired t-tests reported only as detectability indicators at this sample size).

These additions are described in the Methods in Sect. 2.5.1 (Lines 294–302) and Sect. 2.5.2 (Lines 333–335), and the quantitative outcomes are reported in Sect. 3.5 (Lines 641–664) and summarized in Fig. 11 (new) and Tables S6–S7 (new).

The results show that inferred winter-afternoon fluxes at PY are robust to these STILT setup choices: increasing particle number to 1000/2000 changes CO_2ff by −0.56 %/−0.24 % and CO_2tot by −0.52 %/−0.31 %; refining the grid to 0.05° yields similarly small decreases (CO_2ff: −0.72 %; CO_2tot: −0.78 %); and extending the backward duration to 96/120 h produces changes of −1.34 %/−1.05 % (CO_2ff) and −1.33 %/−1.31 % (CO_2tot). Only the intentionally coarser 0.10° grid produces a small but detectable decrease (CO_2ff: −1.47 %; CO_2tot: −1.40 %), while all other settings yield changes ≤1.34 % with 95 % CIs spanning zero. Day-to-day consistency remains essentially unchanged ($r \approx 0.999$; RMSE 0.28–0.45 μmol m^{-2} s^{-1}; Fig. 11; Table S6). CO_2bio shows similarly robust behavior: because wintertime CO_2bio is near zero at PY, we assess it in absolute terms, and the test–baseline differences remain small with 95 % CIs generally spanning zero (Table S7). The across-run day-by-day ensemble spread is also tightly

bounded (median 0.20–0.21 μmol m^{-2} s^{-1}; median CV ≈ 1.8 %), and paired-day scatter remains close to 1:1. Overall, these results indicate that our baseline STILT configuration is in a converged regime and that the inferred winter CO_2ff dominance is robust to reasonable transport-parameter choices. We also made corresponding wording updates in the Abstract and Conclusions to reflect this robustness check (Lines 27–28; Lines 743–746).

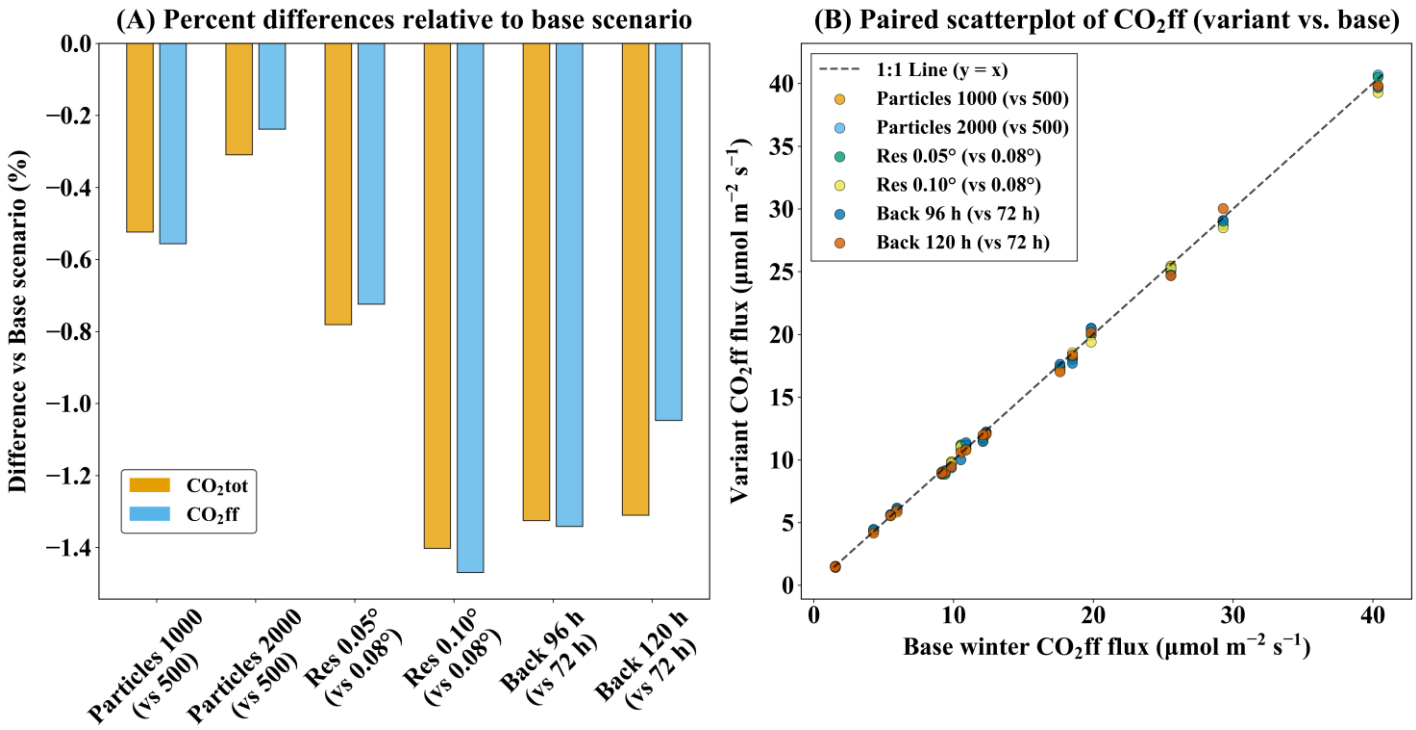

Figure 11. STILT parameter sensitivity at PY (winter). Panel A: mean percent difference (variant − baseline) of inferred fluxes relative to the winter baseline (500 particles, 0.08°, 72 h), computed from paired daily afternoon means (12:00–16:00 LT; n = 18); Δ% = (variant − base)/base × 100; negative values indicate lower than baseline. Panel B: paired scatter of CO_2ff (μmol m^{-2} s^{-1}) from each variant versus the baseline for the same days; solid line is 1:1 (y = x).

Table S6. Wintertime (12:00–16:00 LT) paired-day sensitivity of PY inferred fluxes to STILT parameter choices (n = 18). Variants (particle number, grid spacing, backward duration) are compared with the baseline (500 particles, 72 h, 0.08°). Metrics report effect size (pct_diff_% and 95 % CI), day-to-day consistency (Pearson r), RMSE (μmol m^{-2} s^{-1}), and detectability (paired t-test p value). Upper block: CO_2ff; lower block: CO_2tot. Across the baseline plus six variants, the day-by-day ensemble spread—computed as the standard deviation across the seven runs for each day and then summarized by the median—was 0.20–0.21 μmol m^{-2} s^{-1} (median CV ≈ 1.8%).

metric	comparison	pct_diff_%	pearson_r	rmse	p_value	ci95_lo	ci95_hi
PY_CO_2ff	Back 120 h vs Base (72 h)	-1.05	0.9994	0.38	0.1136	-0.3216	0.0376
	Back 96 h vs Base (72 h)	-1.34	0.9993	0.45	0.0831	-0.3904	0.0265
	Particles 1000 vs Base (500)	-0.56	0.9996	0.33	0.3410	-0.2380	0.0871
	Particles 2000 vs Base (500)	-0.24	0.9995	0.31	0.6738	-0.1916	0.1269

	Res 0.05° vs Base (0.08°)	-0.72	0.9996	0.31	0.1917	-0.2506	0.0542
	Res 0.10° vs Base (0.08°)	-1.47	0.9997	0.39	0.0269	-0.3729	-0.0257
PY_CO_2tot	Back 120 h vs Base (72 h)	-1.31	0.9992	0.44	0.0862	-0.3819	0.0280
	Back 96 h vs Base (72 h)	-1.33	0.9992	0.45	0.0916	-0.3900	0.0322
	Particles 1000 vs Base (500)	-0.52	0.9996	0.28	0.2983	-0.2098	0.0683
	Particles 2000 vs Base (500)	-0.31	0.9995	0.29	0.5502	-0.1864	0.1029
	Res 0.05° vs Base (0.08°)	-0.78	0.9996	0.31	0.1527	-0.2541	0.0431
	Res 0.10° vs Base (0.08°)	-1.40	0.9997	0.35	0.0164	-0.3394	-0.0393

Table S7. Wintertime (12:00–16:00 LT) paired-day sensitivity of PY CO_2bio inferred fluxes to STILT parameter choices (n = 18). Variants (particle number, grid spacing, backward duration) are compared with the baseline (500 particles, 72 h, 0.08°). We report the absolute paired-day test–baseline difference, defined as ΔCO_2bio = CO_2bio(variant) − CO_2bio(baseline), summarized by the paired-day mean (Δ; μmol m^{-2} s^{-1}) and its 95% confidence interval (CI95_lo, CI95_hi; μmol m^{-2} s^{-1}). Because wintertime CO_2bio at PY is close to zero, percent differences are not shown. Across-run daily spread of CO_2bio—defined as the day-by-day standard deviation across the baseline and all variants—has median 0.045 and IQR 0.016–0.067 μmol m^{-2} s^{-1}.

metric	**comparison**	**mean (ΔCO_2bio)**	**ci95_lo**	**ci95_hi**
PY_CO_2bio	Back 120 h vs Base (72 h)	−0.035	−0.094	0.024
	Back 96 h vs Base (72 h)	0.003	−0.057	0.063
	Particles 1000 vs Base (500)	0.005	−0.031	0.041
	Particles 2000 vs Base (500)	−0.009	−0.052	0.033
	Res 0.05° vs Base (0.08°)	−0.007	−0.047	0.033
	Res 0.10° vs Base (0.08°)	0.010	−0.043	0.063

Figure 2: The distinction between the different wind directions is unclear. The authors should consider optimising the figure, for example by using more distinct colours, line styles or annotations, to improve clarity and readability.

Response:

Thanks for the comment. We agree and have revised Fig. 2 to improve separability among wind-

direction sectors and overall readability. Specifically, we (i) adopted a high-contrast, color-blind–friendly palette (Okabe–Ito) for the five sectors (Local/NE/SE/SW/NW), (ii) enhanced marker distinguishability by using uniform symbols with clear edges (white outlines and slight transparency to reduce overplotting), and (iii) moved the legend outside the panels and explicitly labeled the sector angle ranges. These changes substantially improve clarity compared with the previous version. We updated Fig. 2 and its caption accordingly (Lines 349–353).

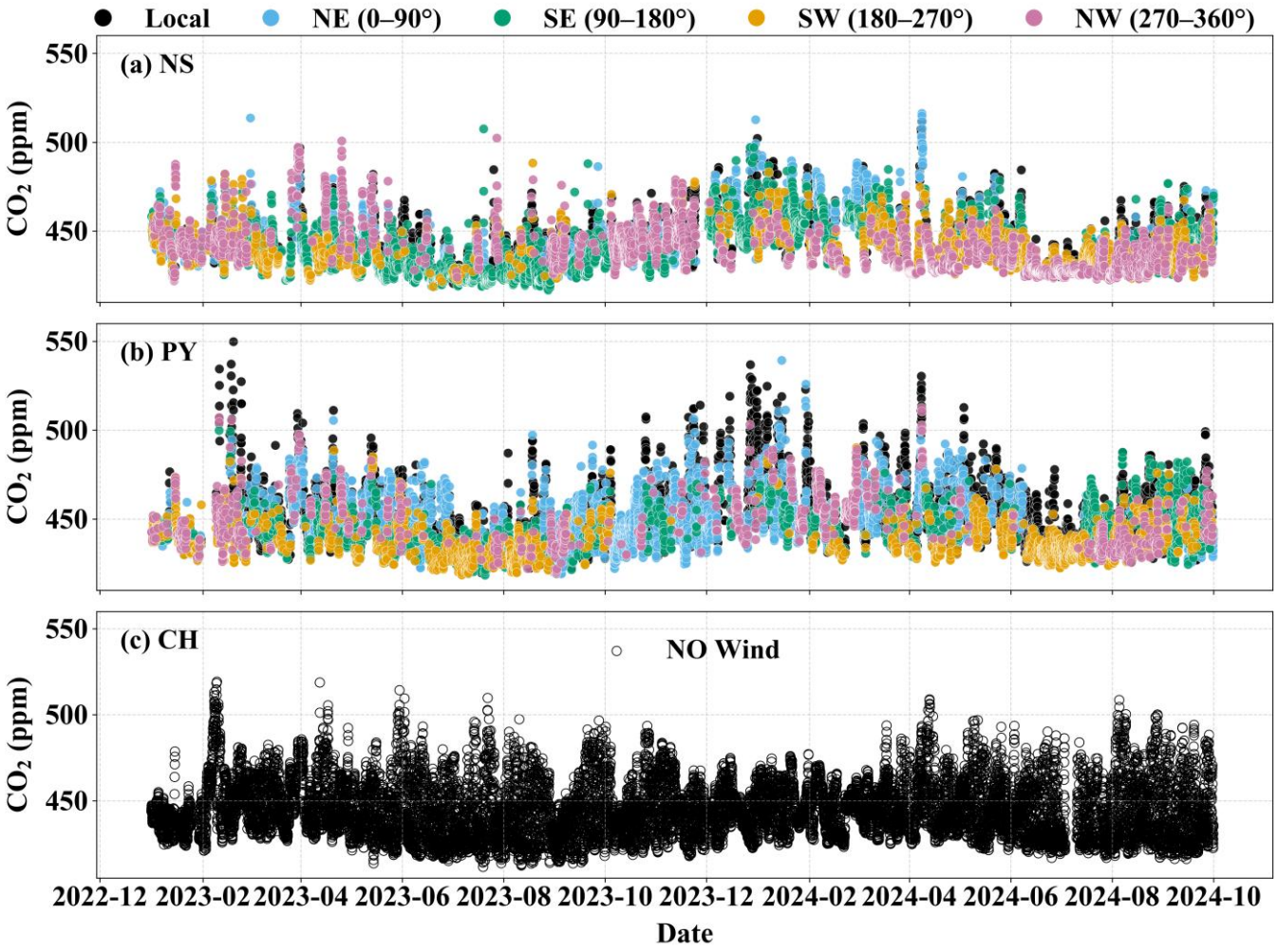

Figure 2. Time series of atmospheric CO_2 concentrations at the (a) NS, (b) PY, and (c) CH stations. For NS and PY, points are color-coded by wind category: local conditions (wind speed < 1.5 m s^{-1}) and four directional sectors for winds ≥ 1.5 m s^{-1} (NE, 0–90°; SE, 90–180°; SW, 180–270°; NW, 270–360°). For CH, wind-direction classification is not shown and the time series is plotted without sector coloring.

Figure 7: It is recommended that the legend be placed outside the figure.

Response:

Thanks for the comment. We have revised Fig. 8 (formerly Fig. 7) by moving the legend outside the figure, as suggested. The time period labels are now placed at the top of the plot for better clarity. We updated Fig. 8 and its caption accordingly (Lines 542–545).

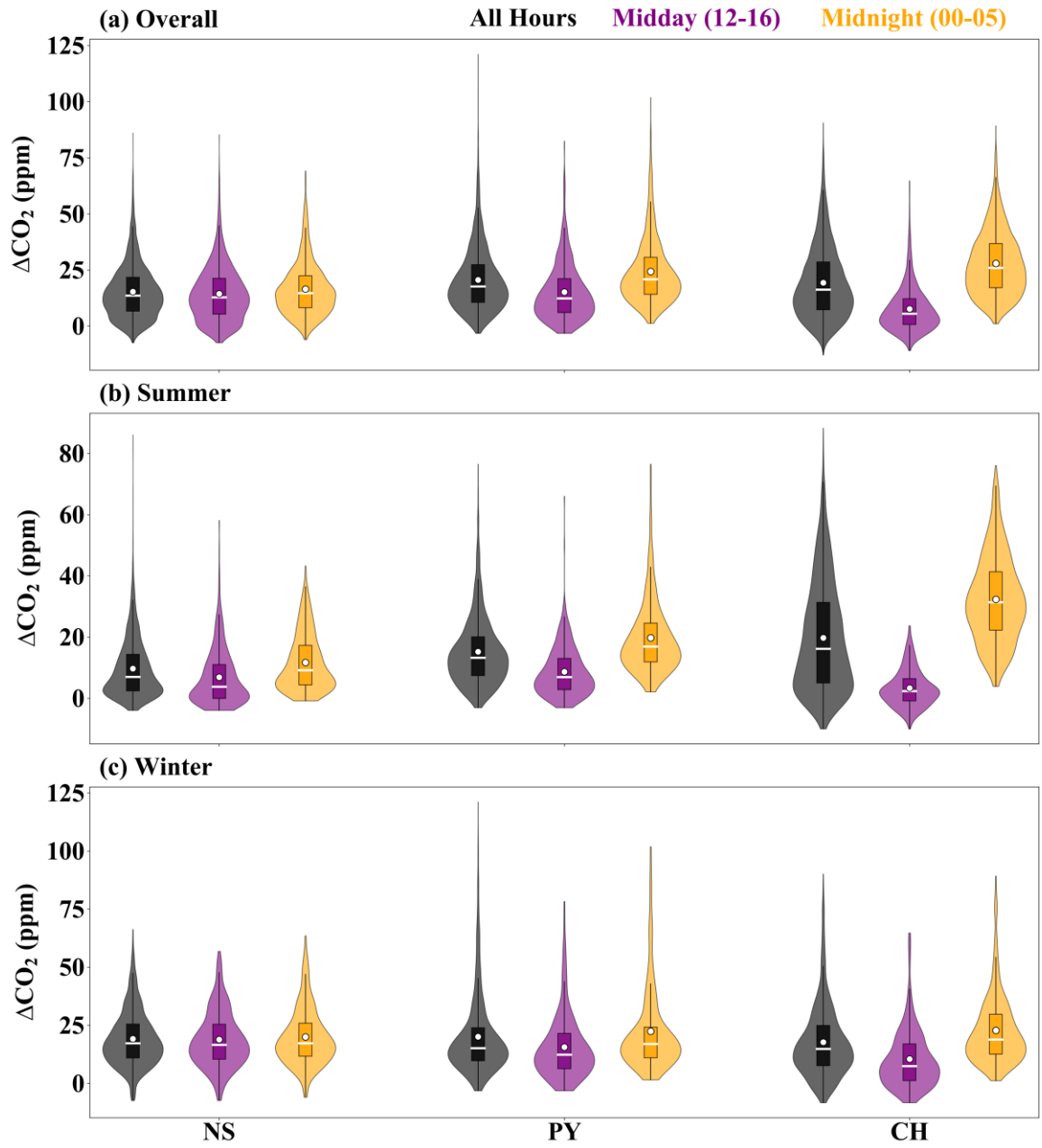

Figure 8. Distributions of hourly CO_2 enhancement (ΔCO_2) above the marine background at NS, PY, and CH during the (a) overall, (b) summer, and (c) winter periods, shown for all hours, midday (12:00–16:00 LT), and midnight (00:00–05:00 LT). White dots denote the mean values, and white horizontal lines denote the median values.

Line 195: ΔCO_2 appears improperly formatted.

Response:

Thanks for pointing out our mistake. We have revised this in Line 265.

On line 288, 'Despite CH's stronger biogenic coupling (NDVI correlation: −0.72; Fig. 3f), NS's CO_2 levels remained 9.80 ppm lower than CH in summer and 5.80 ppm higher in winter, underscoring transport-dominated over biogenic controls at the coastal site.' This whole sentence should be rephrased to enhance

logical rigour.

Response:

Thanks for the comment. We agree that the original wording could be read as conflating CH's strong biogenic coupling with the NS–CH seasonal contrast. We rephrased the sentence to make the logic explicit: CH shows strong biogenic coupling (NDVI–CO_2 correlation −0.72; Fig. 4f), whereas the seasonal sign reversal of NS relative to CH (−9.80 ppm in summer; +5.80 ppm in winter) is more consistent with transport and boundary-layer influences at the coastal site. We support this interpretation by referencing NS's weak NDVI coupling (r = −0.08), narrow NDVI range (0.22–0.42), seasonal shifts in marine–continental transport (summer dilution vs. winter urban outflow) and seasonal boundary-layer depth changes (Figs. 2 and S6). These edits are implemented in Sect. 3.1.1 (Lines 412–417).

On line 324, it states that, at CH, 'smaller daytime weekday–weekend differences suggest that biogenic fluxes outweigh anthropogenic variations'. This statement is somewhat too absolute. It would be better to acknowledge the uncertainties more appropriately and consider the potential influence of atmospheric transport and boundary layer dynamics.

Response:

Thanks for the comment. We agree that the original wording was too definitive. We revised Sect. 3.1.2 (Lines 455–458) to soften the inference and to emphasize that a small weekday–weekend contrast at CH is not a unique indicator of source dominance, because transport and boundary-layer mixing can dilute or mask anthropogenic weekday–weekend signals. We therefore frame this result as a qualitative, supportive observation rather than a standalone attribution diagnostic. For consistency, we also made parallel wording edits for PY and NS to keep the interpretation cautious and process-based across sites (Lines 458–462).